Reports on Progress in Physics

Light-induced electron pairing in a bilayer structure

IOP Publishing Rep. Prog. Phys. 89 (2026) 018003 https://doi.org/10.1088/1361-6633/ae2ba1

Reports on Progress in Physics

PAPER

Light-induced electron pairing in a bilayer structure

Qiaochu Wan[1,*], Daniel Vaz[1], Li Xiang[2], Anshul Ramavath[1], Brandon Vargo[1], Juntong Ye[1], Jonathan Beaumariage[1], Kenji Watanabe[3], Takashi Taniguchi[4], Zheng Sun[5], Dmitry Smirnov[2], Nathan Youngblood[6], Igor V Bondarev[7] and David Snoke[1,*]

[1] Department of Physics and Astronomy, University of Pittsburgh, Pittsburgh, PA 15260, United States of America
[2] National High Magnetic Field Lab, Florida State University, Tallahassee, FL 32310, United States of America
[3] Research Center for Electronic and Optical Materials, National Institute for Materials Science, Tsukuba, Japan
[4] Research Center for Materials Nanoarchitectonics (MANA), National Institute for Materials Science, Tsukuba, Japan
[5] State Key Laboratory of Precision Spectroscopy, East China Normal University, Shanghai, People's Republic of China
[6] Department of Electrical and Computer Engineering, University of Pittsburgh, Pittsburgh, PA 15260, United States of America
[7] Department of Mathematics and Physics, North Carolina Central University, Durham, NC 27707, United States of America
[*] Authors to whom any correspondence should be addressed.

E-mail: qiw74@pitt.edu and snoke@hey.com

OPEN ACCESS

RECEIVED
15 August 2025

REVISED
30 October 2025

ACCEPTED FOR PUBLICATION
11 December 2025

PUBLISHED
21 January 2026

Keywords: excitonic complex, 2D material, charged boson

Supplementary material for this article is available online

Corresponding editor: Dr Lorna Brigham

Abstract

We demonstrate the existence of doubly charged exciton states in strongly screened bilayers of transition metal dichalcogenide layers. These complexes are important because they are preformed electron pairs that can, in principle, undergo Bose–Einstein condensation, in which case they would also form a new type of superconductor, consisting of stable bosons with net charge. Our measurements include 1) continuous control of the doping density with both positive and negative carriers, showing the expected population dependencies on the free carrier density, and 2) measurement of the dependence on magnetic field, showing that this new bound state is a spin triplet. These results imply that it is promising to look for superconductivity in this system.

1. Introduction

Can electrons be paired into bosonic states by any mechanism other than Cooper pairing? Although several mechanisms have been proposed, none has been clearly demonstrated [1–4]. While one might expect that the excess of charge would make this complex unstable due to Coulomb repulsion, a proposal by Yudson [5] showed how the use of light pumping could produce metastable electron pairing by coupling two electrons (or two holes) to an optically-generated exciton, by placing a bilayer structure near a metal layer, as illustrated in figure 1(A). The metal acts to screen out much of the repulsion between like charges. These complexes can be called tetrons [6] or quaternions [7]; here we use the latter term.

In this paper we demonstrate the existence of this type of complex as a stable entity, using some innovations not available at the time of Yudson's paper. By using transition metal dichalcogenide (TMD) layers, which have large (ca. ∼200 meV) exciton binding energy [8], the binding energy of this complex, which is a fraction of the exciton binding energy, can be large compared to k_BT. Also, encapsulating the TMD layers in insulating hexagonal boron nitride (hBN) helps to prevent tunneling current [9]. This experimental observation opens up the possibility of a new type of superconductor that does not involve Cooper pairing. Because they carry two net charges and are also bosonic, they can become a Schafroth superconductor [10]; the theory of BEC–BCS crossover [11, 12] implies that a charged Bose–Einstein condensate is automatically a superconductor.

A metastable state of four fermions in a 2D structure is no longer controversial, in general. In the past decade, numerous reports have confirmed the existence of higher-order excitonic complexes in TMD monolayer and bilayer structures. These include both intralayer and interlayer excitons [13], trions (excitons bound to one extra charge) [14], biexcitons (two neutral excitons bound together) [15], hexcitons (three excitons bound together) [16] and charged biexcitons (biexcitons bound to one extra charge) [15]. The existence of a state with net charge of $2e$, however, has been less well established. Previous work [17] showed evidence of this four-particle bound state, but was limited only to studies of intrinsically doped samples. Here we report definitive confirmation of this excitonic electron pairing. In one set of measurements, the density of the background free charge carriers was continuously varied via gating, which allows the comparison of the relative intensities of the quaternion, trion, and exciton lines. Since the quaternion must add an extra charge to a trion to form, its intensity should increase relative to the trion as the total background charge density increases, just as the trion intensity increases relative to the exciton [18]. A second set of measurements in magnetic field shows that the quaternion species is a spin triplet, with three states $m_J = 0, \pm 1$, as expected by considering the spin structure of the underlying electron and hole states, as opposed to the trion and exciton states, which have just two states that emit light.

2. Experimental methods

Figure 1(B) shows a photograph and figure 1(C) shows the design of the structure used for the electrical gating experiments. The bottom, metallic (Au) layer has two roles; first, it acts as a back gate for the doping of $MoSe_2$ layers, and second, it provides screening that leads to image charge, as shown in figure 1(A). This dual gate structure is aimed to dope the two layers of $MoSe_2$ separately; this structure is commonly used in many interlayer studies [19–21]. We applied the PDMS dry transfer technique to create the stack [22]; the stacks are built on the gold gate with an hBN layer of approximately 2 nm between the TMD layers, a spacer hBN layer of approximately 8 nm between the metal and the first TMD monolayer, and a thick capping hBN layer. The thickness of hBN is determined by AFM after the transfer. Contacts to both $MoSe_2$ layers were then patterned using PMMA for electron-beam lithography, followed by e-beam deposition of 3 nm Ti//25 nm Au to define the drain gate (bottom $MoSe_2$) and the top/source gate (top $MoSe_2$).

As shown in previous theory [17], this image charge is crucial for canceling out much of the like-charge repulsion and making the doubly-charged complex stable. The binding energy of the quaternion is highly dependent on the thickness of the bottom h-BN (d) and the middle h-BN (l). As discussed in this prior work [17], the energy of the quaternion PL line can be higher or lower than the trion energy, depending on the bottom hBN thickness, because its extra charge makes it very sensitive to the screening effect of the metal layer. It is crucial aspect to have thin hBN layers encapsulating all of the TMD monolayers; these insulating layers should be thin enough to allow Coulomb interaction between layers while thick enough to prevent tunneling current. The thickness of the hBN layers in all cases was known within an uncertainty of ± 1 nm.

The vertical gating allows us to vary the free charge density in the bilayer region continuously. When the background charge is negative, an exciton can be bound to two free electrons, while if the background is positive, an exciton can bind to two free holes. The intrinsic doping for the $MoSe_2$ is n-type [23]; therefore we are able to observe the negatively-charged quaternion PL peak with no applied gate voltage.

There was an offset in the open-circuit voltage caused by the intrinsic doping so that the structures had an asymmetric $I - V$ current characteristic (see Supplemental Material). Electrical contact to the bottom $MoSe_2$ was grounded, acting as a drain, and the top gate contacting the top $MoSe_2$ layer could have an applied voltages like a source. This source-drain configuration allowed us to vary the charge in the bilayer without obscuring the imaging of the sample, or changing the asymmetric screening effect of the metallic back gate.

For the magnetic field experiments, a similar structure was used, also with $MoSe_2$ but without the electrical contacts, as illustrated in figure 1(D). The top layer of $MoSe_2$ was an n-type monolayer doped with rhenium. In all experiments, the structures were cooled to approximately 10 K, and optically pumped non-resonantly with a wavelength short compared to the PL emission.

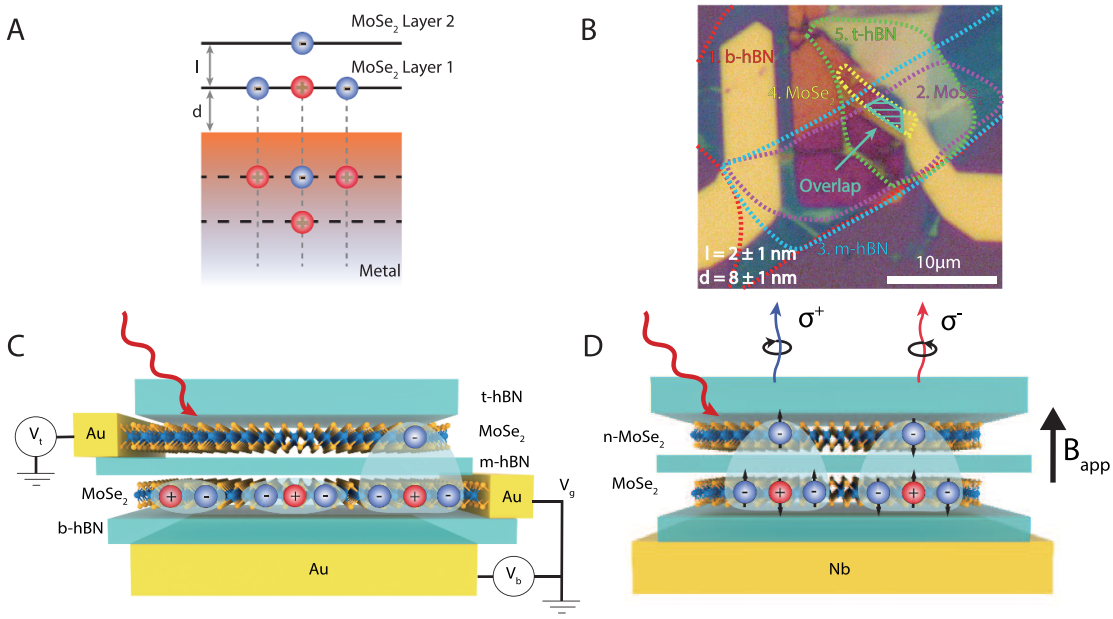

Figure 1. Sample design: (A) Illustration of the quaternion four-fermion state, with image charge in the metal layer. (B) Microscope image of the quaternion sample. (C) The design of the structure, showing the circuit connections, with the middle layer defined as the ground. (D) Geometry of the sample used for the magnetospectroscopy measurements.

3. PL measurement with variable doping

When the structure described above is excited with a laser, an extra PL peak appears between trion and exciton, corresponding to the doubly charged exciton (quaternion) state described above, as seen in earlier work [17]. PL data for the structure of figure 1 is shown in figure 2. We applied voltages on both gates of our sample to tune the doping level on the different $MoSe_2$ layers. The quaternion intensity and trion intensities change dramatically with doping level. We measured the PL with 532 nm green laser pump. For figures 2(A), we only changed the back gate voltage. For figures 2(C) and (D), we fixed the back gate voltage and swept the top gate voltage.

As seen in these figures, the relative intensities of the quaternions, trions and excitons varied significantly with varying doping levels. Figure 2(A) illustrates how the PL spectrum varies as the back gate voltage is varied while the top gate is kept grounded. As the overall negative doping density in the bilayer structure is increased, the intensities of trion and quaternion peaks increase, indicating that, like the trion, the quaternion is a charged complex. We note also that the spectral position of the quaternion line does not shift with voltage. This is expected because the photon emission from the quaternion comes from an electron and hole within a single layer. This behavior clearly distinguishes the quaternion from an interlayer exciton, which has a PL line energy that strongly depends on the electric field between the two layers, because the emitted photon comes from an electron and hole that reside in different layers [19, 24]. Prior work in a very similar sample has shown that the interlayer exciton line appears at much lower energy [19, 25].

Figure 3(A) shows the ratio of the quaternion intensity to the trion intensity as the gate voltages are varied, and figure 3(B) shows the ratio of the trion intensity to the exciton intensity for the same sweeps. The ratio of the trion intensity to the exciton intensity acts as a direct measure of the carrier density. We can estimate the doping density using the mass-action equation [26]

$$n_{\text{doping}} = \left(\frac{I_T}{I_X}\right) \times \left(\frac{\gamma_X}{\gamma_T}\right) \times \left(\frac{4m_X m_e}{\pi \hbar^2 m_T}\right) \times k_B T e^{-E_{Tb}/k_B T}.$$

According to previous studies, we know $m_X = 0.35m_0$ and $m_e = 0.74m_0$ [27, 28]. The decay ratio γ_X/γ_T can be estimated as 6.7, and the energy difference between exciton and trion E_{Tb} is about 30 meV [29, 30]. At around 50 K, we can estimate the doping density varies from $10^{10}\,\text{cm}^{-2}$ to $10^{12}\,\text{cm}^{-2}$.

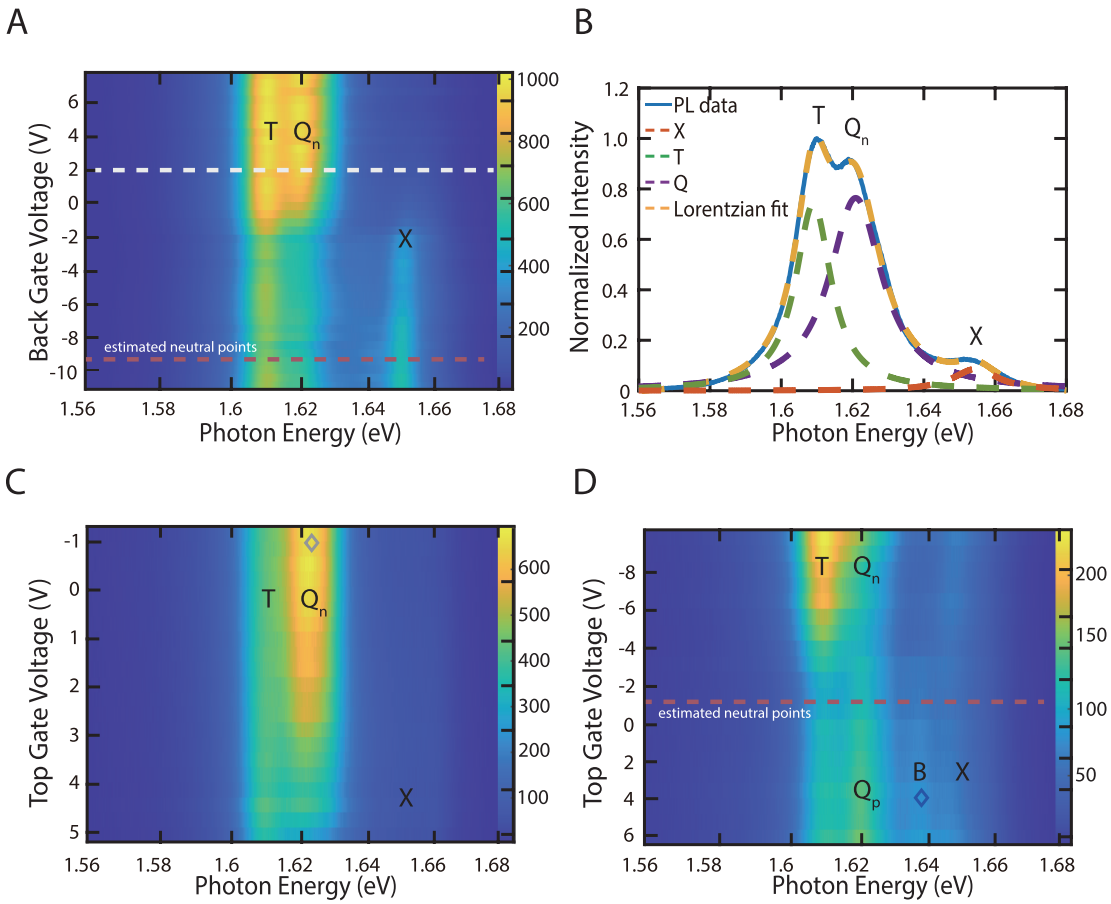

Figure 2. PL measurements with variable doping: (A) PL intensity with back gate sweep; the top gate was set to $V = 0$. The doubly charged exciton peak, labeled Q_n, appears between the trion and exciton lines. (B) PL spectrum for a back gate voltage of +2 V and top gate voltage of 0 V. This PL is a slice from the white dashed line shown in (A). (C) PL with top gate sweep and V_B is fixed to+4 V. The camel color dash line is the estimated neutral points by trion/exciton intensity ratio. (D) PL with top gate sweep and V_B is fixed to−5 V. In this case, the trion and quaternion lines reach a minimum, and then increase as positive versions of both appear when the bilayer region is hole-doped. The bath temperature in all of these cases was 5.5 K. (The diamond symbols in (C) and (D) give the conditions for the intensity-dependence measurements of figures 3(C) and (D), respectively.) The estimated doping density in all of these data varies from $10^{10}\,\mathrm{cm}^{-2}$ to $10^{12}\,\mathrm{cm}^{-2}$, as discussed in the text.

The trion line increases relative to the exciton as the background carrier density increases, in accordance with this mass-action equation. We observe that the quaternion line increases relative to the trion line under the same conditions, which means that it also obeys a similar mass-action equation, relative to the trions; this proves that it has more charge than the trion. At high gate voltage, the curves in figures 3(A) and (B) both saturate, presumably due to nonradiative Auger-like processes.

As seen in figure 2(D), we can switch between negative and positive quaternions in a single sweep as the sign of the background carriers is changed; between these two limits, there is a range around top gate voltage of −2 V with almost zero quaternion density; in this voltage range there are very few background carriers to pick up. We also see in this figure a weak biexciton line [31], which is distinguishable from the quaternion line. As seen in figure 3(D), the intensity of this biexciton line increases quadratically with pump power, as expected since biexciton creation is a two-photon process. By contrast, as seen in figure 3(C), the Q line intensity is linear with pump power, until high density, where it saturates. This shows clearly that the Q line is not a biexciton state. All of our measurements are still within the low-density regime, unlike, for example, recent experiments at high doping and high magnetic field, which presented evidence for six and eight particle states [32].

4. Magneto-optical measurements

In addition to the above doping-dependent measurements, we have measured the magnetic-field dependence of the photoluminescence (PL) of these complexes. As discussed above, a *n*-type sample with rhenium doping was used, without electrical contacts. Using formula above, the doping density of Re is estimated to be about $2 \times 10^{12}\,\mathrm{cm}^{-2}$. The magnetic field was applied out-of-plane and swept from −12

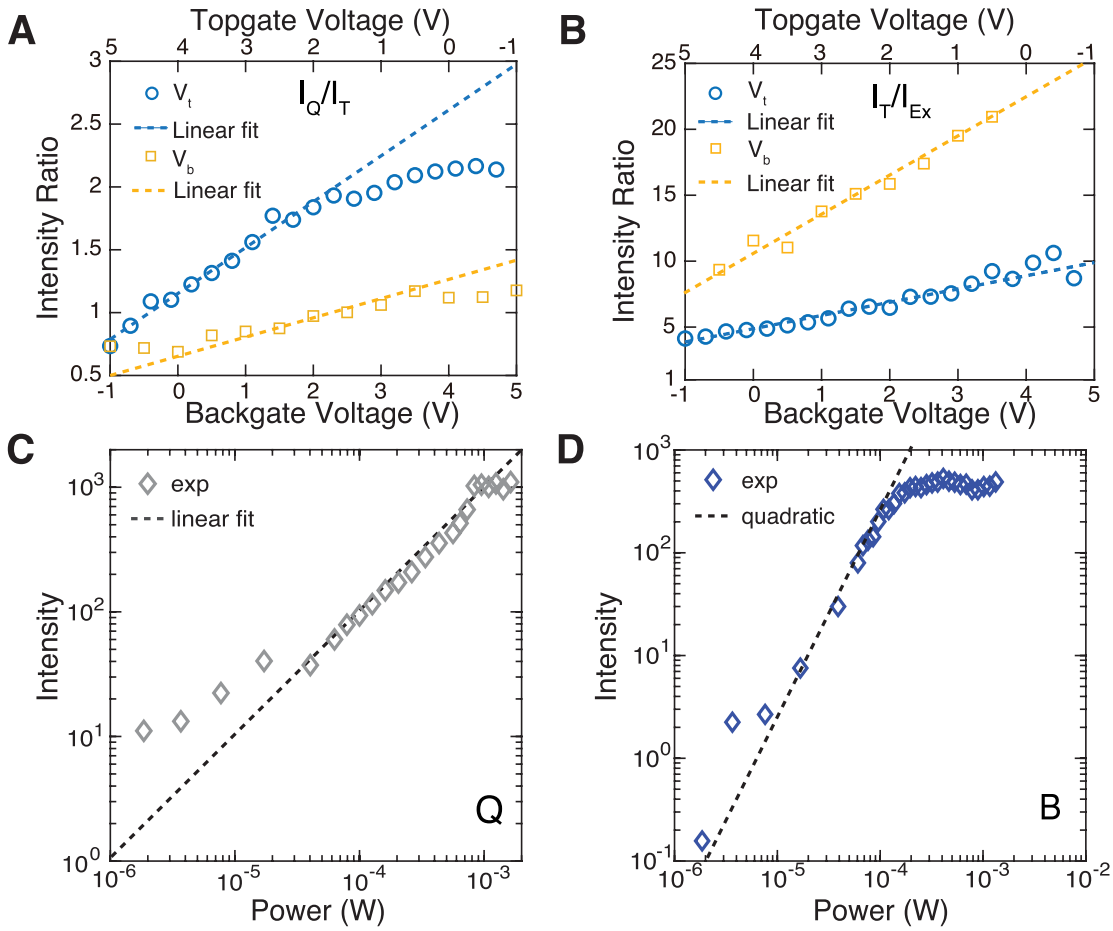

Figure 3. Voltage and power dependent behavior: (A) Ratio of the integrated intensity of the quaternion line to that of the trion line as the gate voltages are swept, at constant pump intensity. (B) Ratio of the integrated intensity of the trion line to that of the exciton line, for the same voltage sweeps as in (A). (C) Quaternion intensity as a function of pump power, for $V_t = -1\,V$ and $V_b = 4\,V$ (shown as the gray diamond symbol in figure 2(C)). (D) Biexciton intensity as a function of pump power, for $V_t = 4\,V$ and $V_b = -5\,V$ (shown as the blue diamond symbol in figure 2(D).)

to +12 Tesla, and the PL was measured for both circular-polarized components. (The pump polarization was right-circular, but since it was far above the exciton energy, the polarization of the injected carriers was almost certainly lost to scattering processes.) figure 4(A) shows the spectrum in the range of the intralayer PL emission as a function of magnetic field for the right-handed polarization (co-circular with the pump), and figure 4(B) shows the data under the same conditions for left-handed circular polarization.

Several effects are immediately observable in these figures. First, the exciton, biexciton, and trion all have linear shifts with magnetic field as previously observed [33–35]. Second, the quaternion line has PL consistent with a spin triplet, with all three states having allowed photon emission. In this sample, the quaternion line appears below the trion line, consistent with earlier observations [17] that the Q line energy is a strong function of the thickness of the bottom hBN layer, which affects the screening from the metal of the back gate. As seen in figures 4(A) and (B), the quaternion line does not have a simple linear shift. Instead, as shown in figure 4(D), the quaternion shifts can be fit to three lines corresponding to the linear field dependences of $m_J = \pm 1$ states that only appear on one side in each of the polarization-resolved images, and a weak quadratic field dependence of the $m_J = 0$ state that appears on the opposite side and emits equally with both circular polarizations of greatly reduced intensity. This behavior is consistent with the selection-rule analysis given in appendix A. Figure 4(C) shows simulated data which is simply the sum of the right-circular $m_J = 1$ line, which shifts with magnetic field, plus the non-shifting $m_J = 0$ weighted by 50% as predicted by the group selection-rule analysis, with each line weighted by a Maxwellian thermal occupation factor, which makes the lower energy range much brighter. The right-circular emission does not appear above the $m_J = 0$ line because it is thermally suppressed by the Maxwellian factor. For the same reason, we also do not see evidence of a singlet $m_J = 0$ quaterion line at higher energy.

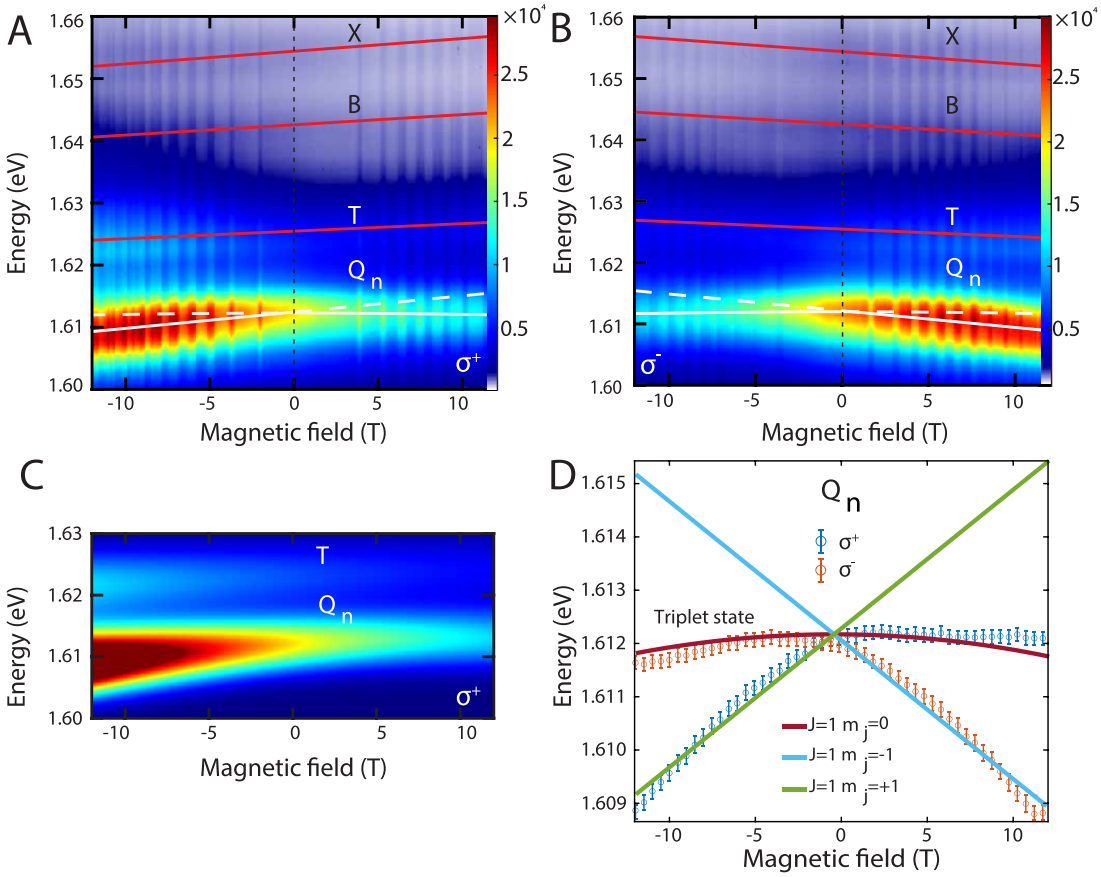

Figure 4. Magneto-PL measurements: (A) PL spectrum as a function of magnetic field for a right-circular polarized emission. (The vertical striations correspond to laser intensity fluctuations.) X: exciton line; T: trion line; B: biexciton line, Q: quaternion line. The white lines indicate linear shifts of the lines with magnetic field. (B) PL spectrum for left-circular polarized PL for the same conditions, with the slopes of the line shifts, but time reversed $B \rightarrow -B$. (C) Simulated data for the right-circular emission from the quaternion triplet, using the linear energy shifts shown in (A) above, weighted by the Maxwellian occupation factor e^{-E/k_BT}, with $T = 29$ K, and line width of 4.6 meV. (D) Composite fit of the full theory (discussed in appendix B) to the peak energies of the Q line extracted from the right- and left-handed data of (A) and (B).

These results, and the identification of the Q line as a quaternion, are consistent with a straightforward theory based on the configuration-space method of calculating the binding energies of the excitonic complexes. The same method gives the experimentally confirmed binding energies for both the interlayer trions and for biexcitons in TMD materials [36], and has also been able to explain the evidence for a positive/negative trion binding energy difference [37]. In prior work [17] we used this method to calculate the quaternion binding energy with the additional inclusion of the image charges in the metal layer. The details of the magnetic field effect analysis, which gives the theory curves plotted in figure 4(D), are given in the appendix B, but the essential results needed to understand the quaternion line shifts are straightforward. First, the ground state of the trion has a hole with two electrons in the same spin state. (We consider here the case of an *n*-doped system, corresponding to the sample used in the magnetic field measurements.) This makes the trion an overall spin-1/2 complex. Next, this intralayer trion is a stable 'core' which is attached to an electron in the other monolayer, to form the quaternion complex. The total quaternion complex therefore is comprised of two spin-1/2 entities, forming triplet and singlet states.

The ground state of this quaternion complex is the triplet state, consistent with the well-known empirical Hund's rule of atomic physics [38]. This rule states that an atomic state with the greatest possible value of the total spin S (for the given electron configuration) and the greatest possible value of angular moment L (for this S) is the one that has the lowest eigenenergy. As an example, in a system of two electrons their total spin can be either 0 or 1. Spin 1 corresponds to a symmetric spin wave function and an antisymmetric coordinate wave function. Since the latter has a node, the probability of finding the two electrons close together is smaller in their triplet state than in the singlet one. This makes their

electrostatic repulsion smaller and the eigenenergy lower compared to that of the singlet configuration. Similarly, for a system of several electrons, the most antisymmetric coordinate wave function corresponds to the greatest spin and the lowest eigenenergy. This applies directly to our quaternion system as well, in which in the triplet configuration the electron of the top layer prefers to stay as far as possible from the trion electrons in the bottom layer, so that their repulsion energy is less.

From the above analysis, the primary shifts of the states will be linear Zeeman-type terms, but as shown in figure 4(D), the full theory presented in appendix B gives a weak quadratic magnetic field dependence of the $m_J = 0$ quaternion state. While this dependence is weak, the fits to the line positions are consistent with the full theory.

5. Discussion and outlook

These experimental results present a highly convincing case for the existence of doubly charged excitons, a.k.a. quaternions, in these specially designed TMD bilayer structures. The doping density and magnetic field experiments give unique signatures for this state which agree well with theory.

These are therefore preformed electron pairs that can possibly undergo Bose–Einstein condensation (BEC) at high density or low enough temperature, and such a BEC state would also be a superconductor. We do not expect this state should emit coherent light, however, as is the case for excitonic and polaritonic condensates. In the case of an excitonic or exciton-polariton condensate, the center-of-mass wave function maps directly to the momentum of an emitted photon. In the case of quaternions, the photon emission leaves behind two electrons and therefore does not map directly to the center of mass of the whole complex. Although we have increased the excitation density of our pump laser, we have not seen evidence for coherent light emission, for example, in spectral line narrowing. Experiments are presently under way to measure electron drag between the two TMD layers, and temperature dependence of the conductivity.

Condensation and the consequent superconductivity will be favored at low temperature. In these experiments the effective temperature of the quaternion gas tends to get hotter due to the excess energy put into the system by the non-resonant pump, which in turn raises the critical density needed for Bose condensation. At high density, nonradiative collisional Auger recombination may also become important; there is evidence for this in figures 3(C) and (D). Both of these effects could be reduced by better cooling the sample; for example, in an immersion flow cryostat as opposed to the cold-finder cryostats used in these experiments. Also, it may be beneficial to laterally confine the carriers in a trap, as done, e.g. for polaritons in [39].

Technically, true BEC is not possible in one and two dimensions [40], but it can often be the case that the coherence length of a two-dimensional Bose system is large compared to the system size. In general, in any finite system in which the size of the system is small compared to the coherence length, the system can undergo a transition indistinguishable from BEC [41, 42], which means it is reasonable to look for superfluidity of the charged bosons in this system. Another fascinating possibility is that since these complexes have long-range Coulomb repulsion, they could form a bosonic Wigner crystal at low temperature, and in principle, could even become a supersolid. The process of Wigner crystallization is controlled by the ratio of the Coulomb repulsion energy over the average kinetic energy of an ensemble of charged particles [43, 44]. Due to their double charge and quadruple mass as compared to electrons, this ratio is almost 10 times greater for quaternions, suggesting much higher quaternion Wigner crystallization temperature than that of the order of 10 K recently observed for quasi-2D electrons in TMD nanostructures [19, 45].

The establishment of quaternion complexes in bilayer systems with metal screening layers opens up a promising field of research, with the real possibility of finding a new, non-BCS type of superconductivity.

Data availability statement

The data that support the findings of this study are openly available at the following URL/DOI: https://doi.org/10.5281/zenodo.16879210.

Supplementary material available at: https://doi.org/10.1088/1361-6633/ae2ba1/data1.

Acknowledgments

We thank Zhehao Dai and Hassan Alnatah for helpful conversations.

Funding

This research is supported by the U.S. Army Research Office Grant No. W911NF-24-1-0237. Z S also wants to acknowledge the National Natural Science Foundation of China (12174111). K W and T T acknowledge support from the JSPS KAKENHI (Grant Numbers 20H00354 and 23H02052) and World Premier International Research Center Initiative (WPI), MEXT, Japan. The magneto-optical measurements supported by the US Department of Energy (DE-FG02-07ER46451) were performed at NHMFL, which is supported by the NSF Cooperative Agreement (Nos. DMR-1644779 and DMR-2128556) and the State of Florida.

Author contributions

Qiaochu Wan 0000-0003-4877-9722
Data curation (lead), Formal analysis (lead), Project administration (lead), Resources (equal), Software (equal), Supervision (equal), Validation (equal), Visualization (equal), Writing – original draft (equal), Writing – review & editing (equal)

Daniel Vaz 0000-0003-2095-7590
Conceptualization (equal), Data curation (equal), Formal analysis (equal), Funding acquisition (equal), Investigation (equal), Methodology (equal), Validation (equal), Visualization (equal), Writing – original draft (equal), Writing – review & editing (equal)

Li Xiang 0000-0002-1565-0271
Data curation (equal)

Anshul Ramavath 0009-0007-3341-636X
Methodology (equal)

Brandon Vargo 0009-0000-3020-271X
Methodology (equal)

Juntong Ye 0009-0002-3755-2282
Methodology (equal)

Jonathan Beaumariage 0009-0004-7500-2999
Methodology (equal)

Kenji Watanabe 0000-0003-3701-8119
Methodology (equal)

Takashi Taniguchi 0000-0002-1467-3105
Methodology (equal)

Zheng Sun 0000-0002-5209-2563
Conceptualization (equal), Writing – original draft (equal), Writing – review & editing (equal)

Dmitry Smirnov 0000-0001-6358-3221
Conceptualization (equal), Resources (equal), Supervision (equal)

Nathan Youngblood 0000-0003-2552-9376
Writing – original draft (equal), Writing – review & editing (equal)

Igor V Bondarev 0000-0003-0739-210X
Conceptualization (equal), Formal analysis (equal), Funding acquisition (equal), Investigation (equal), Project administration (equal), Supervision (equal), Validation (equal), Visualization (equal), Writing – original draft (equal), Writing – review & editing (equal)

David Snoke 0000-0001-8207-6524
Conceptualization (equal), Data curation (equal), Formal analysis (equal), Funding acquisition (equal), Methodology (equal), Project administration (lead), Supervision (equal), Validation (equal), Visualization (equal), Writing – original draft (equal), Writing – review & editing (equal)

Appendix A. Group theoretical analysis of the spin structure

The eigenstates and selection rules of 2D materials have often been analyzed in terms of pseudospin, but it is instructive here to analyze the states in terms of the full group theory. As discussed in [46], the full symmetry group of TMD monolayers in Koster notation is D_{3h}. At the K-valleys which correspond to the lowest energy gap, the symmetry is reduced to C_{3h}. Here, for definiteness, we will stick to the case of positive trions and quaternions, which corresponds to the p-doped sample.

The conduction band states at the K and K' points of the Brillouin zone arise from the z^2d-orbital, and are Γ_2 and Γ_3 in C_{3h} symmetry, while the topmost valence band states arise from the $(x \pm iy)^2 d$-orbital states, and are Γ_1 in C_{3h} symmetry. When electron spin is included, the lowest conduction band states become $\Gamma_{11} \oplus \Gamma_{12}$ (spin projection $m_J = \pm\frac{3}{2}$), and the topmost valence states become Γ_7 and Γ_8 (spin projection $m_J = \pm\frac{1}{2}$). Since each of these is a singly degenerate 1×1 representation in C_{3h}, the multiplication rules are simple: the two bright exciton states correspond to $\Gamma_8 \otimes \Gamma_{12} = \Gamma_5$ and $\Gamma_7 \otimes \Gamma_{11} = \Gamma_6$, which are written as the product states

$$\begin{aligned} &|-\tfrac{1}{2}\rangle|+\tfrac{3}{2}\rangle, && m_J = +1 \quad (K \text{ valley}) \\ &|+\tfrac{1}{2}\rangle|-\tfrac{3}{2}\rangle, && m_J = -1 \quad (K' \text{ valley}). \end{aligned} \tag{1}$$

There are also two 'dark' A-excitons corresponding to $\Gamma_8 \otimes \Gamma_{11} = \Gamma_2$ and $\Gamma_7 \otimes \Gamma_{12} = \Gamma_3$, written as

$$\begin{aligned} &|+\tfrac{1}{2}\rangle|+\tfrac{3}{2}\rangle, && m_J = +2 \\ &|-\tfrac{1}{2}\rangle|-\tfrac{3}{2}\rangle, && m_J = -2, \end{aligned} \tag{2}$$

which cannot emit single photons.

The lowest-energy intralayer trion states are formed by adding another carrier to the A-exciton state, corresponding to $\Gamma_5 \otimes \Gamma_8 = \Gamma_7$ (spin up, in C_{3h}) and $\Gamma_6 \otimes \Gamma_7 = \Gamma_8$ (spin down, in C_{3h}); for example, for a positive trion:

$$\begin{aligned} &|-\tfrac{1}{2}\rangle|+\tfrac{3}{2}\rangle|-\tfrac{1}{2}\rangle, && m_J = +\tfrac{1}{2} \quad (K \text{ valley}) \\ &|+\tfrac{1}{2}\rangle|-\tfrac{3}{2}\rangle|+\tfrac{1}{2}\rangle, && m_J = -\tfrac{1}{2} \quad (K' \text{ valley}). \end{aligned} \tag{3}$$

Each of these emits a photon with the same handedness as an A-exciton in the same valley.

Quaternions are formed of a spin-$\frac{1}{2}$ trion in the bottom layer and an extra spin-$\frac{1}{2}$ carrier in the adjacent top layer, which comes from the opposite K-valley. The multiplication rules for these states in C_{3h} are $\Gamma_7 \otimes \Gamma_7 = \Gamma_5$ ($m_J = +1$), $\Gamma_8 \otimes \Gamma_8 = \Gamma_6$ ($m_J = -1$), $\Gamma_7 \otimes \Gamma_8 = \Gamma_1$, and $\Gamma_8 \otimes \Gamma_7 = \Gamma_1$, but for the last two states, which both belong to 1×1 representations, the rules for time-symmetric states [47] require that we use the Clebsch–Gordan coefficients for symmetric and antisymmetric combinations of the two products, namely $(1/\sqrt{2}, 1/\sqrt{2})$ and $(1/\sqrt{2}, -1/\sqrt{2})$. For a positive quaternion, the three $J = 1$ states are therefore written as follows:

$$\begin{aligned} &\left(|-\tfrac{1}{2}\rangle|+\tfrac{3}{2}\rangle|-\tfrac{1}{2}\rangle\right)|+\tfrac{1}{2}\rangle, && m_J = +1 \\ &\tfrac{1}{\sqrt{2}}\left(|-\tfrac{1}{2}\rangle|+\tfrac{3}{2}\rangle|-\tfrac{1}{2}\rangle\right)|-\tfrac{1}{2}\rangle + \tfrac{1}{\sqrt{2}}\left(|+\tfrac{1}{2}\rangle|-\tfrac{3}{2}\rangle|+\tfrac{1}{2}\rangle\right)|+\tfrac{1}{2}\rangle, && m_J = 0 \\ &\left(|+\tfrac{1}{2}\rangle|-\tfrac{3}{2}\rangle|+\tfrac{1}{2}\rangle\right)|-\tfrac{1}{2}\rangle, && m_J = -1. \end{aligned} \tag{4}$$

As can be seen from this analysis, the two states with $m_J = \pm 1$ emit photons of 100% circular polarization, left- or right-handed ones, while the $m_J = 0$ state produces photons of both handednesses with 50% weight each. As with the trions, the energy of the emitted photon depends on the energy of the two remaining electrons. These have opposite spins for the two $m_J = \pm 1$ quaternions, and a superposition of aligned spins with $m_J = \pm 1$ for the $m_J = 0$ quaternion. In addition to the spin-triplet quaternion, there is also a spin singlet at higher energy, corresponding to the antisymmetric superposition

$$\tfrac{1}{\sqrt{2}}\left(|-\tfrac{1}{2}\rangle|+\tfrac{3}{2}\rangle|-\tfrac{1}{2}\rangle\right)|-\tfrac{1}{2}\rangle - \tfrac{1}{\sqrt{2}}\left(|+\tfrac{1}{2}\rangle|-\tfrac{3}{2}\rangle|+\tfrac{1}{2}\rangle\right)|+\tfrac{1}{2}\rangle, \qquad m_J = 0. \tag{5}$$

This will also be 50% allowed to emit either handedness of polarization. All of these bright states and their spin structures have been illustrated in figure 5, for the p-doped $MoSe_2$ bilayer system. While these states emit photons through intralayer recombination, there are other configurations that were predicted

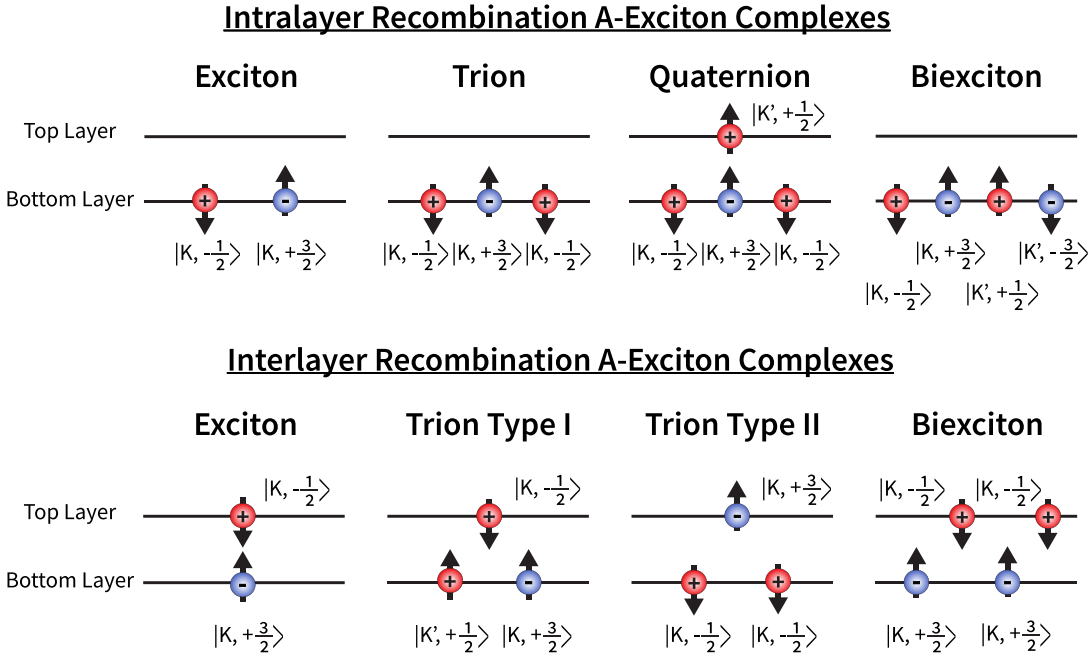

Figure 5. Illustration of the possible bright bound states found in bilayer TMD systems, which have been theoretically predicted [36, 37] and experimentally observed [48–50]. Each of these complexes also has states with other angular momentum values as discussed in the text of appendix A.

[36, 37] and were observed experimentally afterwards [48–50] to recombine through interlayer transitions as seen in figure 5.

We can also examine the spin structure of these indirect transitions, that is, the interlayer transitions. The $m_J = \pm 1$ quaternion states in (4) are forbidden to emit single photons corresponding to a hole in one layer and electron in the other layer, but the $m_J = 0$ state can emit such a photon. There is evidence for this in the very weak line seen at low energy, labeled as Q' in figure S5 of the Supplemental Material. There will also be two allowed emission lines with $J = \pm 1$ corresponding to a single exciton made of a hole in one layer and an electron in the other layer, which is the standard indirect exciton. Finally, an interlayer trion is also possible, consisting of an exciton in one layer and a free electron in the other layer. Indirect emission is possible from two such trion states,

$$\begin{aligned} \left(|-\tfrac{1}{2}\rangle|+\tfrac{3}{2}\rangle\right)|-\tfrac{1}{2}\rangle, \qquad & m_J = +\tfrac{1}{2} \\ \left(|+\tfrac{1}{2}\rangle|-\tfrac{3}{2}\rangle\right)|+\tfrac{1}{2}\rangle, \qquad & m_J = -\tfrac{1}{2}. \end{aligned} \tag{6}$$

Here both electrons correspond to the same K-valley but different monolayers. Both the interlayer exciton and interlayer trion states have emission that shifts with B-field similarly to the intralayer versions. Only the quaternion $m_J = 0$ state does not have this linear shift.

Finally, we look at the spin structure of a biexciton made of two A-excitons in the same layer. The ground state has two excitons of opposite spin [51], corresponding to $\Gamma_5 \otimes \Gamma_6 = \Gamma_1$, which has terms of the form

$$\left(|+\tfrac{1}{2}\rangle|-\tfrac{3}{2}\rangle\right)\left(|-\tfrac{1}{2}\rangle|+\tfrac{3}{2}\rangle\right), \qquad m_J = 0. \tag{7}$$

Either of the two excitons can emit a photon. When a photon is emitted, the final state is an exciton of the opposite handedness. The energy of the photon is therefore the difference between the unshifted biexciton and the exciton energy shifted by magnetic field, which gives an energy shift of the emitted photon.

Appendix B. Theoretical model for the quaternion energy shifts

To elucidate the behavior of quaternion states observed in magnetostatic field experiments, we constructed a theoretical framework based on the spin-Hamiltonian formalism. This approach was originally pioneered by Landau, Gor'kov and Pitaevski, Holstein and Herring, in their studies of molecular

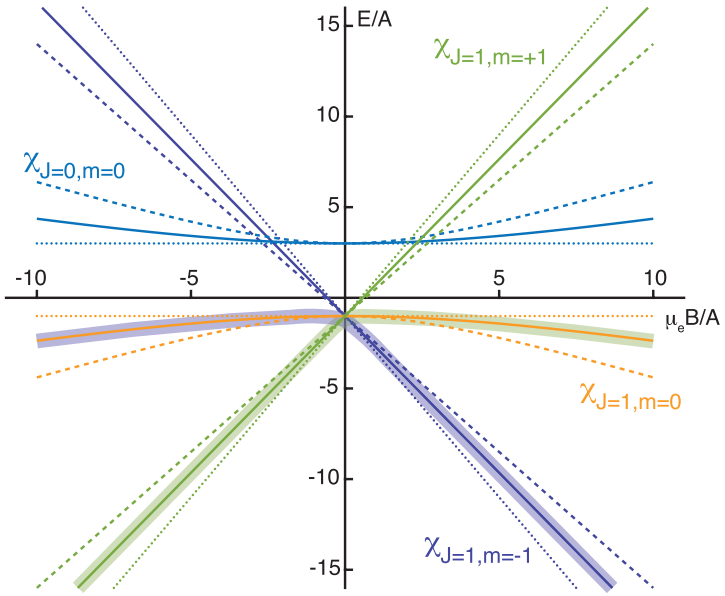

Figure 6. Theoretical prediction of the magnetic field dependence of the quaternion spin states: Triplet (orange, green, purple) and singlet (blue) quaternion energy levels with their respective eigenvectors marked in a constant magnetic field of both orientations as given by equations (13)–(16) for $\zeta = 0.5, 0.73$ and 1 shown by dashed, solid and dotted lines, respectively. The green and purple bands indicate the lowest energy quaternion states that emit photons of right and left circular polarizations respectively as discussed in the previous section.

binding and magnetism [38, 52]. This approach provides a foundational understanding of a broad spectrum of physical phenomena, including nuclear magnetic resonance and electron spin resonance effects [53]. Its foundation was laid back in the 1950's by titans such as Anderson [54, 55], Feynman [56] and Herring [52, 57]. They applied this method to study the hyperfine splitting of the ground state of atomic hydrogen, hydrogen molecular ion and hydrogen molecule as well as collective spin phenomena in solids [58]. A complicated total Hamiltonian is not necessary to analyze the behavior of a complex molecular type entity in a constant magnetic field. Utilizing the stepwise averaging of all the operators of coordinates and momenta in it, apart from the spin operators involved, it can be reduced to an effective spin Hamiltonian to grasp the essence of the Zeeman effect on the system [38].

We consider our quaternion complex being built of the spin-1/2 intralayer trion in a bottom monolayer coupled to a spin-1/2-like charge carrier in the top monolayer, consistent with both spin-structure analysis in the previous section and earlier works [17, 36, 37]. Considering the negative quaternion for definiteness, we have a negatively charged four-particle complex closely resembling the hydrogen, muonium or positronium atoms, with the only difference that its nucleus (trion) is negatively charged while its stability is supported by image charges in the metallic substrate. The spin-Hamiltonian for this negative quaternion system can be obtained from the spin-Hamiltonian of the hydrogen atom in a constant magnetic field, reviewed in full detail in [56], by merely reversing the sign of the proton magneton and the sign of the positive hyperfine splitting constant there, which is proportional to the product of the electron and proton charges. By relabeling the terms accordingly, one then obtains

$$\hat{H} = -A\boldsymbol{\sigma}_e \cdot \boldsymbol{\sigma}_T + \mu_e \mathbf{B}\cdot\boldsymbol{\sigma}_e + \mu_T \mathbf{B}\cdot\boldsymbol{\sigma}_T . \tag{8}$$

Here, A and $\mu_{e,T} = (g_{e,T}/m_{e,T})\,\mu_B$ are the positive constants to represent the electron-trion hyperfine (spin-spin) coupling and their respective magnetic moments with their effective masses (in units of the free electron mass m_0) and g-factors included, $\mu_B = |e|\hbar/(2m_0c) = 0.0579$ meV T^{-1} is the Bohr magneton, and $\boldsymbol{\sigma}_{e,T} = (\sigma_x, \sigma_y, \sigma_z)_{e,T}$ are the Pauli matrices of the electron and trion spin-1/2 subspaces,

$$\sigma_{x_{e,T}} = \begin{pmatrix} 0 & 1 \\ 1 & 0 \end{pmatrix}, \quad \sigma_{y_{e,T}} = \begin{pmatrix} 0 & -i \\ i & 0 \end{pmatrix}, \quad \sigma_{z_{e,T}} = \begin{pmatrix} 1 & 0 \\ 0 & -1 \end{pmatrix}. \tag{9}$$

With the z-quantization axis directed along the magnetic field $\mathbf{B}$ and the general spin-state wave function

$$|\chi\rangle \quad = \quad C_1|+\rangle_e|+\rangle_T + C_2|+\rangle_e|-\rangle_T + C_3|-\rangle_e|+\rangle_T + C_4|-\rangle_e|-\rangle_T,$$

$$|+\rangle = \begin{pmatrix} 1 \\ 0 \end{pmatrix}, \qquad |-\rangle = \begin{pmatrix} 0 \\ 1 \end{pmatrix}, \tag{10}$$

where the C_i for $i=1$ through 4 are unknown coefficients, the matrix of the spin-Hamiltonian (8) takes the following form

	$\lvert+\rangle_e\lvert+\rangle_T$	$\lvert+\rangle_e\lvert-\rangle_T$	$\lvert-\rangle_e\lvert+\rangle_T$	$\lvert-\rangle_e\lvert-\rangle_T$
$\lvert+\rangle_e\lvert+\rangle_T$	$-A+\mu$	0	0	0
$\lvert+\rangle_e\lvert-\rangle_T$	0	$A+\mu'$	$-2A$	0
$\lvert-\rangle_e\lvert+\rangle_T$	0	$-2A$	$A-\mu'$	0
$\lvert-\rangle_e\lvert-\rangle_T$	0	0	0	$-A-\mu$

(11)

with

$$\mu = (1+\zeta)\,\mu_e B, \quad \mu' = (1-\zeta)\,\mu_e B, \quad \zeta = \frac{\mu_T}{\mu_e} = \frac{g_T}{g_e}\frac{m_e}{m_T} = \frac{g_T}{g_e}\frac{m_e}{m_h+2m_e}, \tag{12}$$

where the electron g-factor and electron–hole effective masses can be obtained from the literature, $g_e \approx 2.5$ [59], $m_e \approx 0.88$, $m_h \approx 0.74$ [27], yielding $g_T \approx 5.18$ from Zeeman shift reported [35], to give an estimate $\zeta \approx 0.73$, accordingly. On diagonalization we get the following set of eigenvalue problem solutions (eigenvalues and eigenvectors):

$$\begin{aligned} E_{1,2} &= -A \pm \mu, & |\chi_{1,2}\rangle &= |\pm\rangle_e|\pm\rangle_T = |\chi_{11,1-1}\rangle, \\ E_{3,4} &= A\left(1 \mp 2\sqrt{1+x^2}\right), & |\chi_{3,4}\rangle &= C_\pm|\chi_{10}\rangle \mp C_\mp|\chi_{00}\rangle, \end{aligned} \tag{13}$$

with

$$x = \frac{|\mu'|}{2A} = \frac{|1-\zeta|}{2}\frac{\mu_e B}{A}, \tag{14}$$

where

$$|\chi_{10,\,00}\rangle = \frac{1}{\sqrt{2}}\left(|-\rangle_e|+\rangle_T \pm |+\rangle_e|-\rangle_T\right) \tag{15}$$

and

$$C_\pm = \sqrt{\frac{1}{2}\left(1 \pm \frac{1}{\sqrt{1+x^2}}\right)}, \quad |C_+|^2 + |C_-|^2 = 1. \tag{16}$$

Here, for convenience, the normalized spin eigenfunctions are also written in the form $|\chi_{Sm_s}\rangle$ to indicate the actual spin configurations. The triplet with $S=1, m_s=\pm1,0$ is the ground state and the singlet with $S=0$, $m_s=0$ is the excited state, as shown in figure 6. The compound electron-trion system is assumed to be in the s-state of its relative orbital motion, whereby the quantum number S herein is equal to the total angular moment J of the previous section.

References

[1] Lozovik Y E and Yudson V I 1976 *Sov. Phys. JETP* **44** 389–97
[2] Crépel V and Fu L 2022 *Proc. Natl Acad. Sci.* **119** e2117735119
[3] von Milczewski J, Chen X, Imamoglu A and Schmidt R 2024 *Phys. Rev. Lett.* **133** 226903
[4] Cao J and Kavokin A 2023 *Mater. Today Commun.* **37** 107293
[5] Yudson V I 1996 *Phys. Rev. Lett.* **77** 1564–7
[6] Hadizadeh M, Yamashita M T, Tomio L, Delfino A and Frederico T 2013 *Phys. Rev. A* **87** 013620
[7] Moskalenko S A and Snoke D W 2000 *Bose-Einstein Condensation of Excitons and Biexcitons and Coherent Nonlinear Optics With Excitons* (Cambridge University Press)
[8] Chernikov A, Berkelbach T C, Hill H M, Rigosi A, Li Y, Aslan B, Reichman D R, Hybertsen M S and Heinz T F 2014 *Phys. Rev. Lett.* **113** 076802
[9] Britnell L *et al* 2012 *Nano Lett.* **12** 1707–10
[10] Schafroth M 1954 *Phys. Rev.* **96** 1442
[11] Randeria M 1995 Crossover from BCS theory to Bose–Einstein condensation *Bose-Einstein Condensation* ed A Griffin, D W Snoke and S Stringari (Cambridge University Press)
[12] Snoke D W 2020 *Solid State Physics: Essential Concepts* (Cambridge University Press) ch 11
[13] Jiang Y, Chen S, Zheng W, Zheng B and Pan A 2021 *Light: Sci. Appl.* **10** 72

[14] Plechinger G, Nagler P, Kraus J, Paradiso N, Strunk C, Schüller C and Korn T 2015 *Phys. Status Solidi* **9** 457
[15] Li Z *et al* 2018 *Nat. Commun.* **9** 3719
[16] Choi J, Li J, Van Tuan D, Dery H and Crooker S 2023 arXiv:2312.09476
[17] Sun Z *et al* 2021 *Nano Lett.* **21** 7669
[18] Ross J S *et al* 2013 *Nat. Commun.* **4** 1474
[19] Zhou Y *et al* 2021 *Nature* **595** 48–52
[20] Sung J *et al* 2020 *Nat. Nanotechnol.* **15** 750
[21] Wang X *et al* 2021 *Nat. Nanotechnol.* **16** 1208
[22] Castellanos-Gomez A, Buscema M, Molenaar R, Singh V, Janssen L, Van Der Zant H S and Steele G A 2014 *2D Mater.* **1** 011002
[23] Kang J, Tongay S, Zhou J, Li J and Wu J 2013 *Appl. Phys. Lett.* **102** 012111
[24] Szymanska M and Littlewood P 2003 *Phys. Rev. B* **67** 193305
[25] Shimazaki Y, Schwartz I, Watanabe K, Taniguchi T, Kroner M and Imamoğlu A 2020 *Nature* **580** 472–7
[26] Liu Y, Shen T, Linghu S, Zhu R and Gu F 2022 *Nanoscale Adv.* **4** 2484–93
[27] Liu E, van Baren J, Lu Z, Taniguchi T, Watanabe K, Smirnov D, Chang Y-C and Lui C H 2021 *Nat. Commun.* **12** 6131
[28] Mouri S, Zhang W, Kozawa D, Miyauchi Y, Eda G and Matsuda K 2017 *Nanoscale* **9** 6674–9
[29] Rassay S S 2017 Electrical, electronic and optical properties of $MoSe_2$ and WSe_2 *Phd Thesis* Institute of Technology
[30] Lundt N, Cherotchenko E, Iff O, Fan X, Shen Y, Bigenwald P, Kavokin A, Höfling S and Schneider C 2018 *Appl. Phys. Lett.* **112** 031107
[31] Hao K *et al* 2017 *Nat. Commun.* **8** 15552
[32] Van Tuan D, Shi S F, Xu X, Crooker S A and Dery H 2022 *Phys. Rev. Lett.* **129** 076801
[33] MacNeill D, Heikes C, Mak K F, Anderson Z, Kormányos A, Zólyomi V, Park J and Ralph D C 2015 *Phys. Rev. Lett.* **114** 037401
[34] Aivazian G, Gong Z, Jones A M, Chu R L, Yan J, Mandrus D G, Zhang C, Cobden D, Yao W and Xu X 2015 *Nat. Phys.* **11** 148–52
[35] Li Y *et al* 2014 *Phys. Rev. Lett.* **113** 266804
[36] Bondarev I V and Vladimirova M R 2018 *Phys. Rev. B* **97** 165419
[37] Bondarev I V, Berman O L, Kezerashvili R Y and Lozovik Y E 2021 *Commun. Phys.* **4** 134
[38] Landau L D and Lifshitz E M 2013 *Quantum Mechanics: Non-Relativistic Theory* vol 3 (Elsevier)
[39] Balili R, Hartwell V, Snoke D, Pfeiffer L and West K 2007 *Science* **316** 1007
[40] Hohenberg P C 1967 *Phys. Rev.* **158** 383
[41] Bagnato V and Kleppner D 1991 *Phys. Rev. A* **44** 7439
Dai W-S and Xie M 2003 *Phys. Rev. A* **67** 027601
[42] Bondarev I V and Meliksetyan A V 2014 *Phys. Rev. B* **89** 045414
[43] Platzman P M and Fukuyama H 1974 *Phys. Rev. B* **10** 3150
[44] Bondarev I V, Boltasseva A, Khurgin J B and Shalaev V M 2025 arXiv:2503.05165
[45] Smoleński T *et al* 2021 *Nature* **595** 53–57
[46] Xiao D, Liu G B, Feng W, Xu X and Yao W 2012 *Phys. Rev. Lett.* **108** 196802
[47] Koster G F, Dimmock J O, Wheeler R G and Statz H 1963 *Properties of the Thirty-Two Point Groups* (MIT Press)
[48] Jauregui L A *et al* 2019 *Science* **366** 870–5
[49] Kremser M, Brotons-Gisbert M, Knörzer J, Gückelhorn J, Meyer M, Barbone M, Stier A V, Gerardot B D, Müller K and Finley J J 2020 *npj 2D Mater. Appl.* **4** 8
[50] Sun X, Zhu Y, Qin H, Liu B, Tang Y, Lü T, Rahman S, Yildirim T and Lu Y 2022 *Nature* **610** 478–84
[51] Ostatnický T, Gilliot P and Hönerlage B 2005 *J. Appl. Phys.* **98 113516**
[52] Herring C 1962 *Rev. Mod. Phys.* **34** 631
[53] Slichter C P 2013 *Principles of Magnetic Resonance* vol 1 (Springer)
[54] Anderson P W 1950 *Phys. Rev.* **79** 350
[55] Anderson P W and Hasegawa H 1955 *Phys. Rev.* **100** 675
[56] Feynman R P 2010 *The Feynman Lectures on Physics* vol III (Basic books)
[57] Herring C and Flicker M 1964 *Phys. Rev.* **134** A362
[58] Feynman R P 2018 *Statistical Mechanics: A Set of Lectures* (CRC Press)
[59] Oreszczuk K, Rodek A, Goryca M, Kazimierczuk T, Raczyński M, Howarth J, Taniguchi T, Watanabe K, Potemski M and Kossacki P 2023 *2D Mater.* **10** 045019